BOUNDED PLASMA EDGE PHYSICS AS OBSERVED FROM SIMULATIONS IN 1D AND 2D

by

David Cooperberg, Keith Cartwright, and Charles K. Birdsall

Memorandum No. UCB/ERL M96/85

20 December 1996

BOUNDED PLASMA EDGE PHYSICS AS OBSERVED FROM SIMULATIONS IN 1D AND 2D

by

David Cooperberg, Keith Cartwright, and Charles K. Birdsall

Memorandum No. UCB/ERL M96/85

20 December 1996

ELECTRONICS RESEARCH LABORATORY

College of Engineering
University of California, Berkeley
94720

PROLOGUE

This report is a summary of research done by the authors over the past three years or so, to be expanded into more detailed ERL reports and journal submissions, in 1997. A version of this report was presented by Prof. C.K. Birdsall as invited papers at the *International Conference on Plasma Physics* (Nagoya, Japan, Sept. 9-13, 1996) and at the *Double Layer Symposium, Potential Formation and related Nonlinear Phenomena in Plasmas* (Sendai, Japan, Sept. 17-19). That version will appear in the proceedings of the latter conference. The object is to seek the non-neutral plasma edge ($n_i \neq n_e$), sheath and pre-sheath behaviors [time-average, plus oscillations and waves, at both high (electron) and low (ion) frequencies], that occur at the edges of neutral plasmas ($n_i \approx n_e$), including being driven. The tools are analytic modeling plus computer simulations. Comparisons are to be made with laboratory experiments, and applications are to be made to plasma devices. The authors have given talks and poster papers (as progress reports) on some of the material covered in this report, as follows:

X.Q. Xu, G. DiPeso, V. Vahedi, and C.K. Birdsall, "Theory and Simulation of Plasma Sheath Waves," UCB/ERL Memorandum No. M92/148, 15 December 1992.

D.J. Cooperberg, V. Vahedi, C.K. Birdsall, "PIC-MCC with Variable Particle Weights," *Numerical Simulation of Plasmas Conference,* Valley Forge, PA, September 7-9, 1994.

D.J. Cooperberg, C.K. Birdsall, "Particle Simulation of Surface Waves," *American Physical Society, Div. of Plasma Physics Annual Meeting,* Minneapolis, MN, November 7-11, 1994.

K.L. Cartwright and C.K. Birdsall, "Ion Wave Propagation into the Plasma Sheath," *American Physical Society, Div. of Plasma Physics Annual Meeting,* Minneapolis, MN, November 7-11, 1994.

K.L. Cartwright and C.K. Birdsall, "Refraction and Reflection of Ion Acoustic Solitons by Space Charge Sheath," *23rd IEEE International Conference on Plasma Science,* 3-5 June, Boston, Massachusetts, 1996.

D.J. Cooperberg and C.K. Birdsall, "Particle-in-Cell Simulation of Plasma Surface Wave Sustained Discharges," *23rd IEEE International Conference on Plasma Science,* 3-5 June, Boston, Massachusetts, 1996.

C.K. Birdsall, D.J. Cooperberg and K.L. Cartwright, "Waves and Oscillations near the Plasma Edge," (invited paper) *1996 International Conference on Plasma Physics (ICPP '96)* Nagoya, Japan, September 9-13, 1996.

C.K. Birdsall and members of his Plasma Theory and Simulation Group, "Bounded Plasma Edge Physics as observed from simulation in 1d and 2d" (invited, opening talk) *Fifth Symposium on Double Layers, Potential and Related Nonlinear Phenomena,* Sendai, Japan, September 17-19, 1996.

K.L. Cartwright and C.K. Birdsall, "Refraction and Reflection of Ion Acoustic Solitons by Space Charge Sheath," *Fifth Symposium on Double Layers, Potential and Related Nonlinear Phenomena,* Sendai, Japan, September 17-19, 1996.

K.L. Cartwright and C.K. Birdall, "Refraction and Reflection of Ion Acoustic Solitons by Space Charge Sheath formed by a Grid," *American Physical Society Division of Plasma Physics* November 11-14, 1996.

This research has been supported by ONR, with the general title of:

Plasma Boundaries, Neutral and Non-Neutral Plasmas, Plasma Devices

Research supported by:

ONR Contract FD-N00014-90-J-1198 and ASSERTS N00014-94-1-1033, N00014-93-1-1389.

Bounded Plasma Edge Physics As Observed From Simulations in 1d and 2d

David Cooperberg, Keith Cartwright, and Charles K. Birdsall
Electronics Research Laboratory
University of California, Berkeley, CA 94720-1774

Abstract

Part I (DC): Plasmas bounded by conducting or dielectric walls develop sheaths and pre-sheath regions with physics which is distinctly different from that of the bulk plasma, due to large charge separations ($n_i \neq n_e$), large electric fields, and large potentials ($e\phi > kT$, or larger, when driven). One dimensional simulations, at high frequencies (on the order of ω_{pe}), show: (a) plasma oscillations, associated with the bulk; and (b)resonances (dipole, series, Tonks-Dattner, Parker, Nickel and Gould, etc.), associated with the edges. Two dimensional simulations of a plasma slab show wave propagation along the walls (in y) localized in the edge (analogous to Gould-Trivelpiece waves in a plasma column). The resonances found in 1d are the cut-off frequencies ($k_y = 0$) in 2d. Driving the plasma at or near $f_{series} = f_{pe}(2s/L)^{1/2}$ shows the resistive nature of this resonance.

Part II (KC): Low frequency behavior of the plasma edge has also been examined by using ion acoustic waves in the bulk. The resultant perturbed density has provided a sensitive measure of the sheath dynamics as observed in the spatial profiles of densities, fields, potentials, and particle moments. The sheath electric field formation is observed, moving inward from the wall at sound velocity; we postulate formation of IAW's by this "compression", and show subsequent trapping of IAW's in the bulk.

1 Electron Surface Waves

1.1 Introduction to Electron Resonances and Surface Waves in Bounded Plasmas

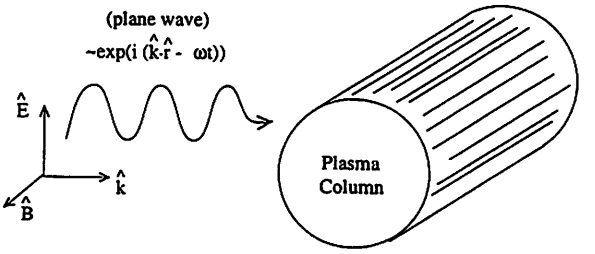

Figure 1: Schematic of experiment to detect electron resonances in a plasma column.

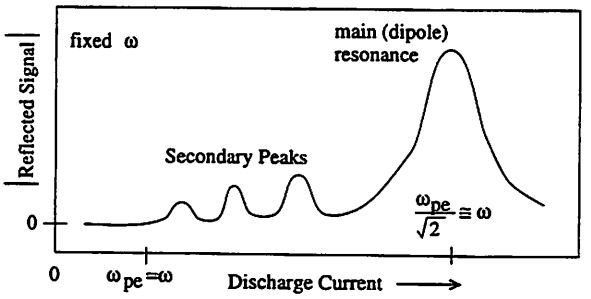

Figure 2: Sketch of scattered field intensity

Electron resonances in bound plasmas have been studied and observed for some time. In 1931 Tonks studied the fields scattered by a plasma column and found that the scattered field versus plasma density exhibits multiple resonances (Figs. 1 and 2). These results were re-derived by Herlofson (1951) in study of ionized meteor tails. A cold homogeneous treatment (Tonks, Herlofson, Vandenplas) of this experiment describes only the main (dipole) resonance. The additional peaks require the presence of thermal electrons (Gould 1960, Vandenplas 1961). These additional resonances are called secondary, thermal or Tonks-Dattner resonances. A more complete explanation of the peak spacing in the resonance spectrum requires inclusion of a plasma radial density profile[1]. Here the resonances may be understood as radial longitudinal standing waves confined in the region between the plasma boundary and the cutoff radius where $\omega = \omega_{pe}(r_c)$.

Taillet[2] describes a resonantly sustained RF discharge in which the discharge is predicted to be sustained by a signal at the main resonance. This discharge was conducted in a planar device (plasmoid) and the main resonance in this configuration is known as the series resonance.

The electron resonances found in a radially bounded plasma represent cutoffs for waves which may propagate in the axial direction. The main and Tonks-Dattner resonances of a plasma column represent cutoffs for surface waves (Trivelpiece???, O'Brien[7]) which propagate along the column axis.

Moisan et. al.[3] has studied HF SW discharges in plasma columns which operate with frequencies of 1MHz to 10GHz. Analytic models for the axial field and plasma dependencies in these SW discharges are being studied (Kortshagen, Aliev, Schlütter, etc...). The EEDF in low pressure SW discharges is being carefully examined. In this regime it has been proposed that collisionless (quasilinear) damping may contribute significantly to the wave absorption and produce a hot electron tail (Aliev et. al.)

1.2 Thermal Electrons, Immobile Ions; Computer Experiment, 2d3v

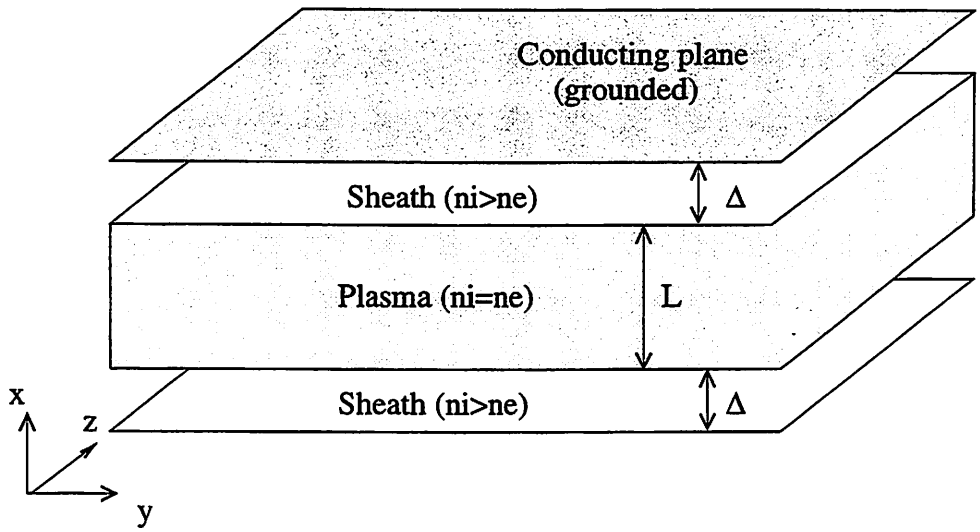

Figure 3: Schematic of plasma slab simulation.

The initial model used to study surface waves in metal bounded plasmas in slab configuration (2d3v) includes a uniform, immobile, neutralizing background of ions and thermal electrons loaded in the center of the region (Fig. 3). The positive sheath regions are modeled as electron free regions of thickness Δ adjacent to the metal boundaries which are maintained by specular reflection of electrons at a distance, Δ, from the walls. This model enabled a detailed comparison between of $\omega(k_y) = \omega_r(k_y) + i\omega_i(k_y)$ and eigenfunctions in $\hat{x}$ as measured in simulation and calculated from the linearized Vlasov equation. (We assume that all wave quantities may be written as $F(x)e^{i(k_y y - \omega t)}$, with k_y real).

The kinetic theory is based on the work of Xu et. al.[4] and Cheng and Harris[5]. The results for the real part of the dispersion relation, in the limit $\Delta \gg \lambda_{De}$, is

$$\omega_r{}^S = \frac{\omega_{pe}}{\sqrt{1+\coth\left(\frac{k_y L}{2}\right)\coth(k_y\Delta)}}\left(1+\frac{\sqrt{3}}{2}k_y\lambda_{De}\sqrt{\tanh\left(\frac{k_y L}{2}\right)\coth(k_y\Delta)}\right). \quad (1)$$

for the symmetric (in the perpendicular, x direction) mode and

$$\omega_r{}^{AS} = \frac{\omega_{pe}}{\sqrt{1+\tanh\left(\frac{k_y L}{2}\right)\coth(k_y\Delta)}}\left(1+\frac{\sqrt{3}}{2}k_y\lambda_{De}\sqrt{\coth\left(\frac{k_y L}{2}\right)\coth(k_y\Delta)}\right). \quad (2)$$

for the asymmetric (in x) branch. When $\Delta \sim \lambda_{De}$, there are significant contributions to the plasma dielectric function

$$\epsilon(\omega, k) = 1 + \frac{\omega_{pe}^2}{k^2 v_{Te}^2}[1 + \zeta Z(\zeta)] \tag{3}$$

from components where $\zeta(= \frac{\omega}{\sqrt{2}kv_{Te}}) \sim 1$, and one must evaluate Z, the plasma dispersion function, explicitly to compute the dispersion relation. Of particular interest is the value of ω for the asymmetric mode in the $k_y = 0$ limit. Equation 2 then reduces to

$$\omega_r{}^{AS} = \sqrt{\frac{2\Delta}{2\Delta + L}}\left(1 + \sqrt{\frac{3\lambda_{De}^2}{2\Delta L}}\right) \equiv \omega_{sr} \tag{4}$$

where ω_{sr} is known as the series resonance.

Results are obtained by analysis of transforms taken in time and space (propagation dimension) of the electrostatic potential in a PIC simulation of a thermally excited plasma in steady-state. The diode length is $L_y = 0.02m$. Figure 4 and 5 show simulation and theoretical results for real dispersion, for the asymmetric and symmetric surface waves and first few body (Bohm-Gross) waves. The "exact" theory shown in Figure 4 refers to a numerical evaluation for ω_r which allows for $\zeta \sim 1$. Figure 6 and 7 show the form of the eigenfunctions describing the transverse dependence of the waves.

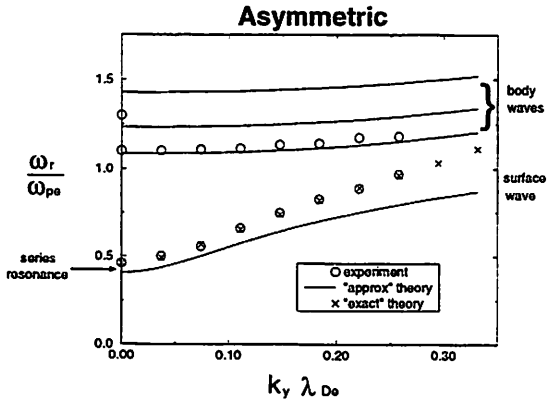

Figure 4: Dispersion relations showing the asymmetric surface wave (lower) and asymmetric Bohm-Gross branches (upper). ω_{pe} is peak value

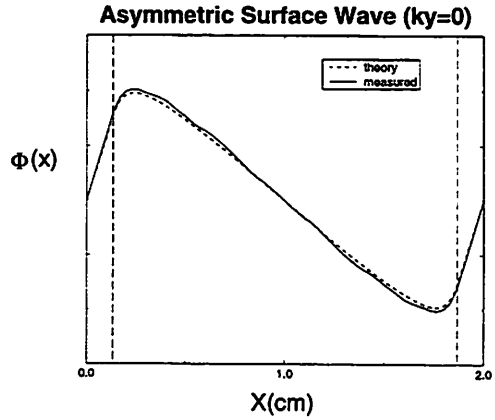

Figure 6: Electron density perturbation (at series resonance).

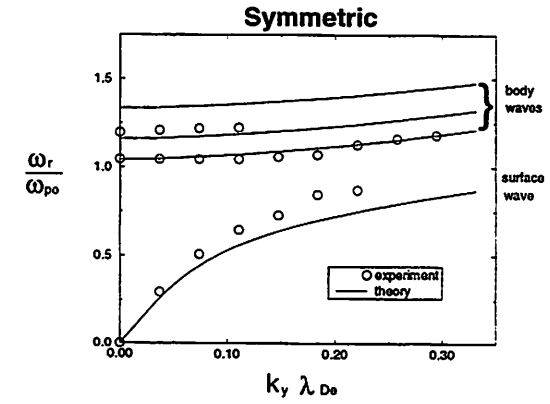

Figure 5: Dispersion relations showing the symmetric surface wave (lower) and symmetric Bohm-Gross branches (upper). ω_{pe} is peak value

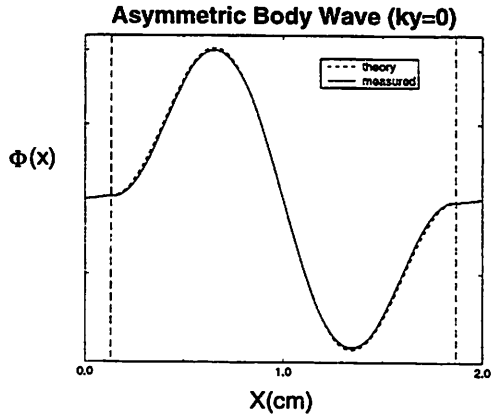

Figure 7: Electron density perturbation (the first, asymmetric, Bohm-Gross (body) wave, $k_y = 0$)

The expression for collisionless Landau damping of these waves is

$$\omega_i = \frac{-D_i(\omega_r, k_y)}{\left.\frac{\partial D_r(\omega,k_y)}{\partial \omega}\right|_{\omega_r}} = \frac{\sum_{k_x=\frac{n\pi}{L}=-\infty}^{\infty} \frac{\epsilon_i(\omega_r,k)}{k^2(\epsilon_r^2(\omega_r,k)+\epsilon_i^2(\omega_r,k))}}{\frac{\partial}{\partial\omega}\left(\sum_{k_x=\frac{n\pi}{L}=-\infty}^{\infty} \frac{\epsilon_r(\omega,k)}{k^2(\epsilon_r^2(\omega,k)+\epsilon_i^2(\omega,k))}\right)_{\omega_r}}. \quad (5)$$

This expression is evaluated numerically and compared with results from computer experiments in Figure 8. No assumptions about ζ are used in evaluating the plasma dispersion function.

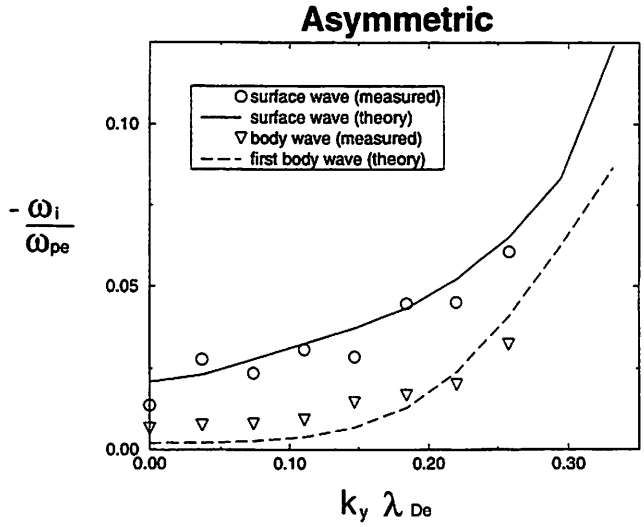

Figure 8: Imaginary part of dispersion relations for the asymmetric surface wave and the first asymmetric Bohm-Gross branch. ω_{pe}. is peak value

In the next section we shall add the effects of a nonuniform ion density profile. This allows for the existence of additional "secondary" surface wave modes.

1.3 Thermal, Nonuniform Plasma; Computer Experiment, 2d3v

Computer simulations of an undriven, 2d3v, thermal, plasma slab have allowed detection of surface waves. These simulations enabled the measurement of the wave dispersion relations and the structure of the surface waves (spatial variation) in the linear regime. A description of the experiment and a summary of results follows.

The plasma slab consists of an ion species (Ar^+) and electrons. Both species are mobile. The plasma density is maintained by creating ion - electron pairs uniformly through the system, as if by photo-ionization, at a constant rate ($\sim 2.5 \times 10^{14}/cm^3 - sec$) chosen to maintain a given peak density. A 1 mTorr background neutral gas (Argon) pressure is maintained to allow, via electron-neutral elastic scattering, a mechanism to mix the electron velocity components (electron-neutral inelastic collisions and ion-neutral collisions are omitted). This is necessary to reduce electron cooling in the perpendicular direction. Ions are created at room temperature while electrons are created at temperatures $\sim 4eV$.

The model described forms a self-consistent sheath and non-uniform density profile (Fig. 9). This system can be compared to the results of a fluid calculation in a manner similar to that of Parker, Nickel, and Gould[1] who describe transverse resonances in an inhomogeneous thermal plasma column. We extend the analysis to include electron momentum transfer collisions and axially propagating waves in a plasma slab. The main, or first symmetric and antisymmetric, modes are analogous to Gould-Trivelpiece[6] waves in a plasma column, while the secondary branches have been studied in the laboratory by O'Brien[7]. The observed cut-off ($k_y = 0$) frequencies for these waves are thought to result from longitudinal waves which are trapped in a surface layer defined by the reflecting potential of the sheath

region on one side and some critical distance inside the plasma at which local plasma frequency equals the wave frequency[6]. Exponential decay of the mode is expected beyond this critical distance.

The linear fluid calculation is performed by substituting the following zero and first order expressions into the electron continuity equation, electron equation of motion, and Poisson's equation.

$$\begin{aligned} n_e &= n_{eo}f(x) + n_1(x)e^{i(k_y y-\omega t)}, & v_e &= v_1(x)e^{i(k_y y-\omega t)} \\ p &= p_o(x) + p_1(x)e^{i(k_y y-\omega t)}, & \Phi &= \Phi_o(x) + \Phi_1(x)e^{i(k_y y-\omega t)} \\ p_o &= n_{eo}f(x)kT_e, & \nabla p_1 &= \gamma kT_e \nabla n_1, \qquad (\gamma = 3) \end{aligned} \tag{6}$$

The electron steady-state density profile $f(x)$ (Fig. 9) is determined by the computer simulation. The resulting differential equation (Eq. 7) is solved numerically to yield the dispersion relations and the eigenfunctions $\Phi_1(x)$. The results are plotted along with values measured in our computer simulation (Fig. 10, 11, 12). In Figures 11 and 12 the critical point, X_c marks the location at which the oscillation frequency equals the local plasma frequency. We expect a decaying solution for $\Phi_1(x)$ from this point towards the center. ω_{pe} and λ_{De} (Eq. 7) are taken at the midplane.

$$\nabla^2\nabla^2\Phi_1 - \frac{1}{\gamma}\left(\frac{\nabla f}{f}\cdot\nabla\right)\nabla^2\Phi_1 + \left[\frac{1}{\gamma\lambda_{De}}\left(\frac{\omega^2}{\omega_{pe}} - f\right) - \frac{1}{\gamma}\nabla\cdot\left(\frac{\nabla f}{f}\right)\right]\nabla^2\Phi_1 - \frac{1}{\gamma}\nabla f\cdot\nabla\Phi_1 = 0 \tag{7}$$

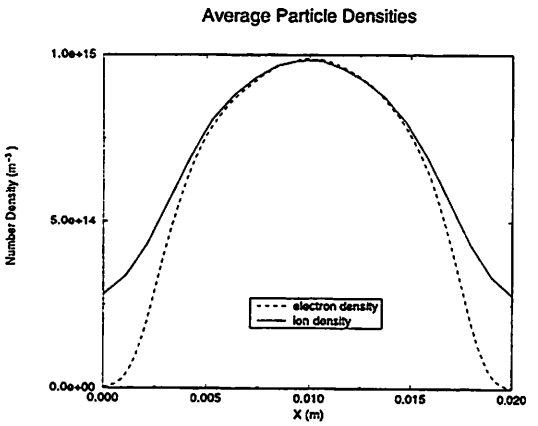

Figure 9: Electron and ion density profiles averaged in time and axial ($\hat{y}$) direction ($L_x = 2.0cm \approx 42\lambda_{De}$).

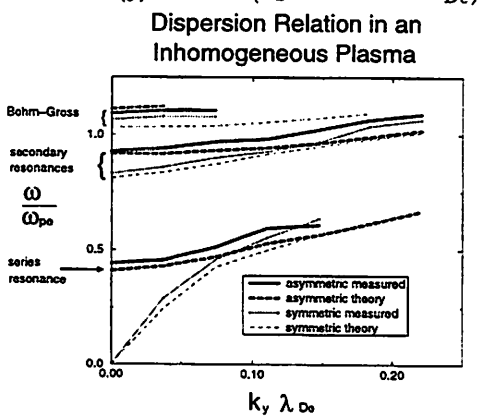

Figure 10: Dispersion relations showing main (lower two) and secondary branches. ω_{pe} is peak value

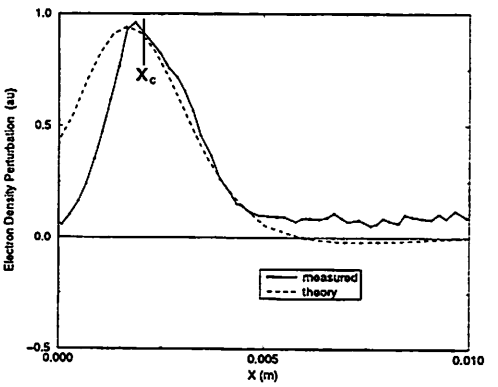

Figure 11: Electron density perturbation from edge to mid-plane of system (at series resonance, $k_y = 0$).

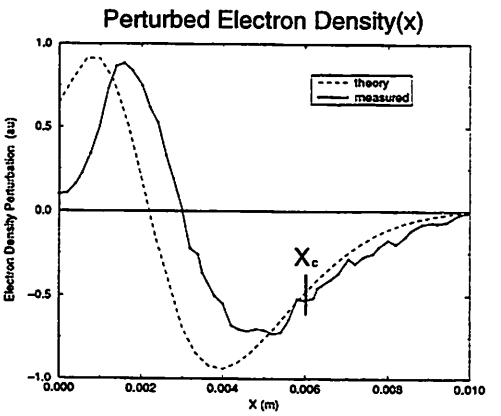

Figure 12: Electron density perturbation from edge to mid-plane of system (the first, asymmetric, secondary branch, $k_y = 0$)

1.4 RF Resonantly Sustained Argon Discharge; Computer Experiment, 1d3v

In this experiment an Argon discharge (1d3v) is sustained by applying a driving voltage signal with a RF frequency located approximately at the series resonance of the plasma slab. It is observed via simulation that an applied signal of fixed frequency can maintain a discharge whose profile yields a series resonance near the applied frequency($\omega_{rf} \approx \omega_{sr}$). Since the plasma impedance approaches a pure resistance at this frequency, exceptionally small applied (low voltage) signals can be used by comparison with conventional capacitively coupled discharges where the diode impedance is nearly pure capacitance.

The computer simulations incorporate an MCC package[8] which includes the following reactions. The previous mechanism of uniform ionization is not needed here since fully self-consistent electron heating and subsequent ionization is modeled.

(1)	$e + Ar$	$\longrightarrow$	$e + Ar$	(Momentum Transfer)
(2)	$e + Ar$	$\longrightarrow$	$e + Ar^*$	(Excitation)
(3)	$e + Ar$	$\longrightarrow$	$e + Ar^+ + e$	(Ionization)
(4)	$Ar^+ + Ar$	$\longrightarrow$	$Ar + Ar^+$	(Charge Exchange)
(5)	$Ar^+ + Ar$	$\longrightarrow$	$Ar^+ + Ar$	(Scattering)

Results of the computer experiments can be compared with the homogeneous 1d model for a capacitive discharge (Godyak[9], Lieberman and Lichtenberg[10]). This analytic model and some of its predictions are summarized below.

The analytic model assumes uniform stationary ions, no electrons in sheath regions, and $n_e = n_i = n_o$ in the central region(Fig. 13). Current is constant through the discharge and is approximately equal to the electron conduction current in the neutral region and the displacement current in the sheath regions. The diode impedance (neglecting low frequency ion contributions), as seen by the voltage source, is then

$$Z(\omega) = \frac{s_1}{i\omega A\epsilon_o} + \frac{s_2}{i\omega A\epsilon_o} + \frac{d}{i\omega A\epsilon_p} \quad (8)$$

$$= \frac{2\bar{s}}{i\omega A\epsilon_o} + \frac{d}{i\omega A\epsilon_p} \quad (9)$$

with

$$\epsilon_p = \epsilon_o \left[1 - \frac{\omega_{pe}^2}{\omega(\omega - i\nu_m)}\right]$$

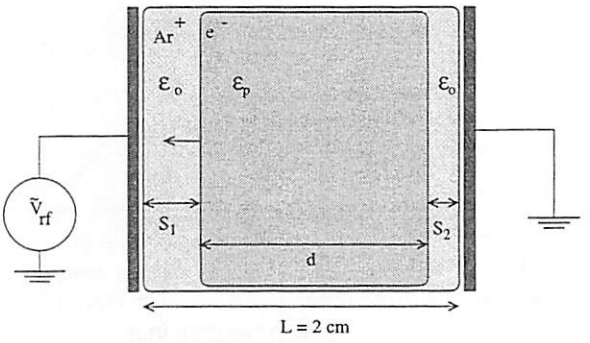

Figure 13: Schematic of the homogeneous model.

Godyak arrived at an expression for plasma density n as a function of the applied frequency and voltage by balancing the outgoing particle flux with ionization which determines the electron temperature and then equating power loss (includes collisional losses, ionization loss, electron KE and ion KE loss) to power absorbed (taken to be $Re(\tilde{V}^2/Z)/2$) to arrive at

$$\frac{\omega_{pe}^2}{\omega^2} = \frac{L}{2\bar{s}}\left[1 \pm \frac{\nu_m}{\omega}\left(\frac{\tilde{V}^2}{V_{min}} - 1\right)^{1/2}\right]$$

Note that $\omega = \omega_{pe}\sqrt{2\bar{s}/L} \equiv \omega_{sr}$ at $\tilde{V} = V_{min}$ or $\nu_m = 0$. Also, from the displacement current in the sheaths,

$$\tilde{I} = -en_o A\frac{ds_{1,2}}{dt} = Re(\frac{\tilde{V}}{Z})$$

with $Z(\omega_{sr}) = \frac{\nu_m m L \epsilon_o}{n_o e^2 A}$, we can solve for $\bar{s}$ and find that

$$\omega = \omega_{pe}\sqrt{\frac{2\left(\frac{eV_{min}}{\omega \nu_m m_e L}\right)}{L}}$$

which produces the scaling law,

$$n \sim \omega^3.$$

This is in contrast to the capacitively coupled RF discharge scaling, $n \sim \omega_{rf}^2$.

A series of experiments at varying ω_{rf} and fixed p_{argon} are described in Table 1 and Figures 14,15, and 16. Some of the notable features common to each of these discharges are summarized here. Applied V lags I by less than 25° so the diodes are essentially resistive. Also, $\nu_m \approx 10^7 T_e(eV) Hz \ll \omega_{source}$, where T_e is average kinetic energy of electrons. A peak potential $\sim 10 V_{source} > V_{ioniz.}$ ($\approx 15eV$) is observed near the plasma boundaries(Fig. 11). The scalings $n \propto \omega^3$ (Fig. 16), $s \propto 1/\omega$ are followed. An extrapolation to $f_{source} = 2450$ MHz produces $n_{epeak} \approx 10^{13}/cm^3$.

Varying ω_{rf}, fixed neutral density

Experiment	f_{source} (Mhz)	p argon $(mTorr)$	V_{source} (V)	$n_{e\,peak}$ (cm^{-3})	$f_{pe\,peak}$ (MHz)	T_e (V)	P (mW/cm^2)
A	110	10.0	2.5	7.2e8	241	3.4	1.9
B	120	10.0	2.5	1.0e9	284	3.4	2.6
C	140	10.0	2.5	1.7e9	370	2.9	3.6
D	200	10.0	2.5	6.2e9	706	2.3	11.
E	300	10.0	3.	1.36e10	1050	2.8	35.
F	400	10.0	3.	4.0e10	1800	2.8	103.
G	470	10.0	3.	7.2e10	2420	3.0	180

Table 1: Parameters for various experiments, $\nu_m(Hz) \approx 10^7 T_e(eV)$. V lags I by less than 25° in case A-G. $\lambda_i(cm) \approx 3.2 p_{gas}(mTorr)$, $k_y = 0$, $L_x = 2cm$ for experiments A–G.

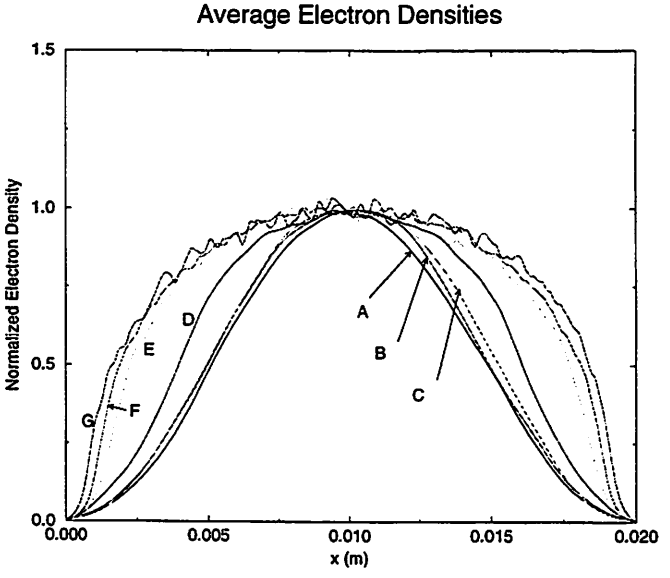

Figure 14: Time-averaged normalized electron densities for cases A-H of Table 1.

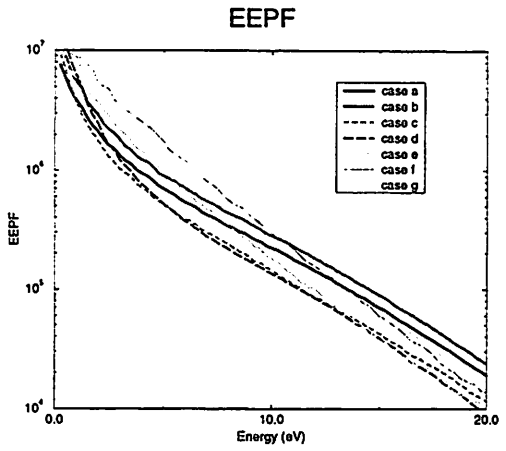

Figure 15: Electron energy probability function (a.u.) for cases A-G of Table 1. Note the presence of a Bi-Maxwellian distribution at frequencies ($p_{argon} = 10mT$).

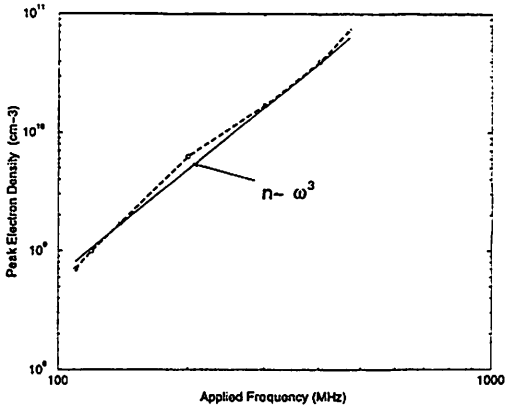

Figure 16: ω_{rf} v. n_{epeak} for fixed n_{argon}.

Another series of experiments was conducted in which p_{argon} was varied with a fixed ω_{rf}. The data are shown in Table 2. The mechanism of electron heating is studied in these simulations. A transition is seen between the low ($\lesssim 100mT$) and high pressure regimes. Figures 17– 20 of the time averaged $J_{electron} \cdot E$ illustrate this transition. The "theory" curve in these plots is generated by modifying the fluid calculations of Section 1.3 to include an electron momentum transfer collision term. At lower pressures, the electron heating profiles show a wave-like structure as a result of the strong resonant surface wave fields. The heating cannot be modeled as Ohmic. At higher pressures, the plasma is well modeled by the collisional fluid equations and the heating is Ohmic.

Figures 22 and 21 show the amplitude and phase of the diode admittance exhibited in a representative discharge at low pressure. The admittance is measured by measuring the response to an applied, low amplitude ($V_{probe} \ll V_{rf}$), probe signal. The main (series) resonance and alternating symmetric and asymmetric secondary resonances are revealed by alternating maxima and minima in Figure 22. The series resonance is observed to be very closely matched to the source frequency.

Here we present a qualitative explanation for the stability and self tuning observe in these resonant discharges. To start our discussion we point out that in all experiments the applied voltage lagged the diode current by between 10° and 25° after the steady-state had been achieved. We also find that the driving frequencies are very close to the series resonance as shown in Figs. 21 and 22. Examination of the homogeneous impedance (Eq. 9) and the inhomogeneous fluid calculations described in Section 1.3 then tell us that the driving frequency must be near but less than the series resonance. With this point established we can quickly explain the stability of these discharges. To proceed we make the further argument that the ion density profile (and also the electron profile under the assumption of quasi-neutrality) can be described by ambipolar diffusion for $\lambda_i \ll L$, where L is the width of the sytem or at lower pressures by a variable mobility model or a langmuir solution[10] (and306ish). In each case the normalized density profile, n/n_{mid}, is given as a function of only $n_{neutral}$, T_e, and T_i. T_i can be approximated by the neutral temperature and T_e is determined by $n_{neutral}$ as a result of particle conservation[10]. The result we are after is that the steady-state normalized density profile, n/n_{mid}, is independent of the power absorbed by the plasma. The result is that an increase(decrease) in absorbed power will bring an increase(decrease) in $n_peak \propto \omega_{sr}$, and, since we have established that these discharges are being operated just below the series resoance, a decrease(increase) in the power dissipated in the plasma (since the resonance has moved further from the drive frequency) which leads to a decrease(increase) in n_peak. The result is a discharge in stable equilibrium whose density is determined by the driving frequency and the neutral gas pressure (and the geometry of the system).

It should also be mentioned that these discharges are aslo stable to high frequency fluctuations. The result for ω_{sr} (Eq. 4)in the homogeneous, thermal model of section 1.2 shows that an increase in T_e

leads to an increase(decrease) in ω_{sr} as before and consequently a stabilizing decrease(increase) in T_e. (mention that peak density is determined by freq. only. - not drive sig amp. – transition?? - min voltage??) (check godyak book- spike curve)(stable equ. M.L.) For sufficiently high Q plasmas (i.e. low pressures) and low applied voltages we find that the peak plasma density is determined by the applied drive freqency and not the drive amplitude. The relation between $V_{applied}$ and $f_{applied}$ is derived for the homogeneous model by Godyak[9].

Varying neutral density, fixed ω_{rf}

Experiment	f_{source} (Mhz)	p argon $(mTorr)$	V_{source} (V)	$n_{e\,peak}$ (cm^{-3})	$f_{pe\,peak}$ (MHz)	ν_m (MHz)	λ_{De} (cm)	T_e (V)	P (mW/cm^2)
H	140	2.0	3.4	8.2e8	256	13	14.	7.1	7.0
I	140	10.0	2.5	1.7e9	370	30	3.8	2.9	3.44
J	140	100.0	3.8	3.0e9	490	260	0.41	2.5	3.9
K	140	300.0	6.0	3.7e9	545	780	0.14	2.5	5.35

Table 2: Parameters for various experiments, $\lambda_i\,(cm) \approx 3.2 p_{gas}\,(mTorr)$, $k_y = 0$ for experiments H–K.

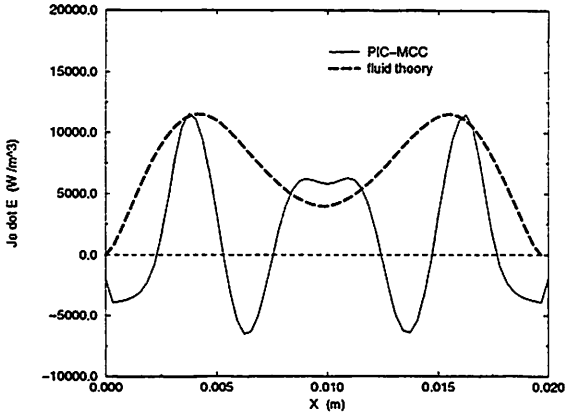

Figure 17: Electron heating profile, $J \cdot E$ ($p_{argon} = 2mT$, case H).

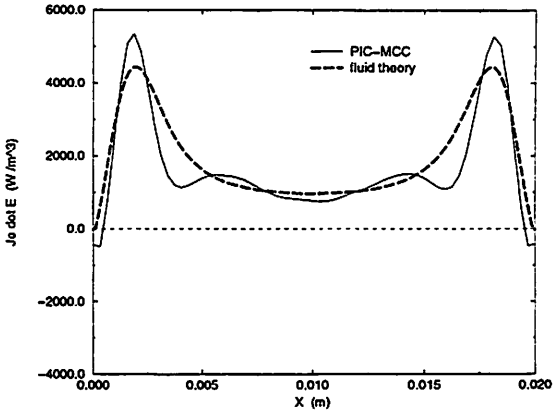

Figure 19: Electron heating profile, $J \cdot E$ ($p_{argon} = 100mT$, case J).

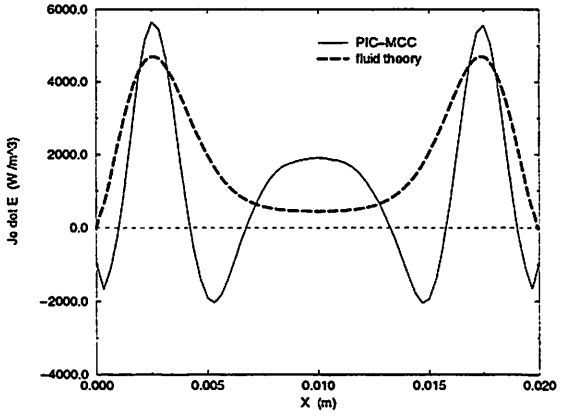

Figure 18: Electron heating profile, $J \cdot E$ ($p_{argon} = 10mT$, case I).

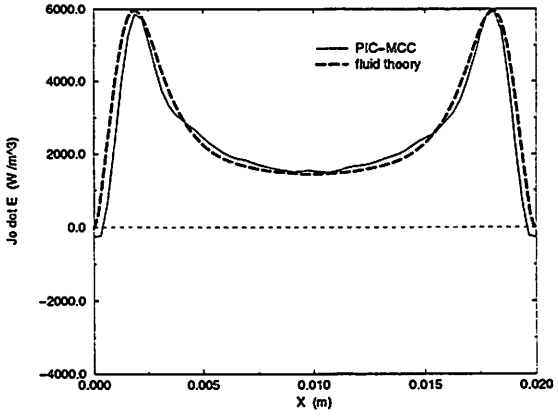

Figure 20: Electron heating profile, $J \cdot E$ ($p_{argon} = 300mT$, case K).

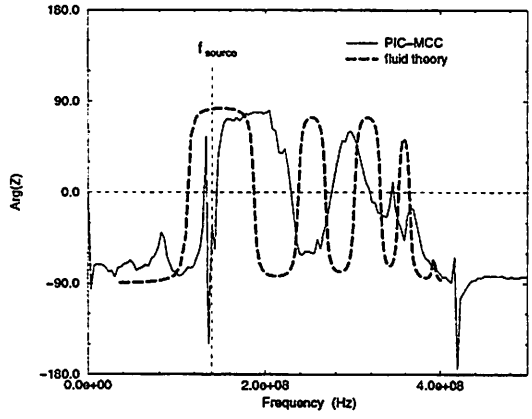

Figure 21: Phase of plasmoid impedance (case-I), f_{drive} = 1.4e8 Hz).

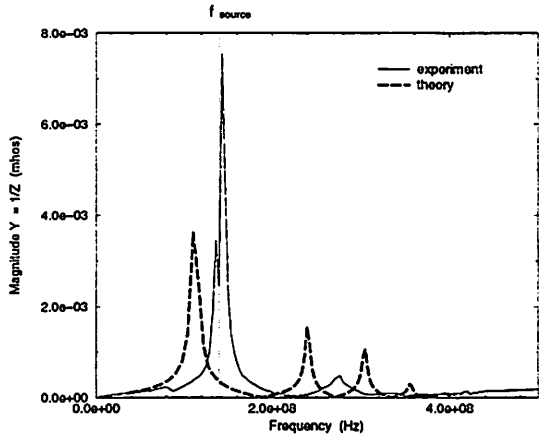

Figure 22: Magnitude of plasmoid admittance (case-I, f_{drive} = 1.4e8 Hz).

It should be noted that while the density and sheath scaling laws predicted by Godyak are in good agreement with our theory, the actual mechanism for electron heating (assumed ohmic in the simple homogeneous model) is not justified in describing the simulations. Our computer experiments at low pressures show particle-wave interactions (Figs. 17 and 18) which produce a hot electron population (Fig. 15).

1.5 Standing Surface Wave Sustained Discharge; Computer Experiment, 2d3v

Electromagnetic standing surface waves have also been used in computer experiments to sustain an Argon discharge in 2d3v. These experiments are similar to the 1d experiments at the series resonance except that we now use a standing wave in a 2d plasma bound by rectangular conducting walls(Fig. 23). The standing wave (Fig. 24) is observed to have an ω and k_y which closely match those predicted by the first antisymmetric mode in the linear, thermal calculation of the previous section. A fully electromagnetic field solve is incorporated in these simulations, where the fields are subcycled, to allow for self-consistent wave formation. Current loop antennae are introduced to drive the system. Discharge parameters are

- $L_x = 2.0cm, \qquad L_y = 8.0cm$
- $f_{rf} = 150MHz, p = 10mT$ Argon
- $n_{epeak} = 2.8 \times 10^9 cm^{-3}$
- $T_e = 3.5eV$

The field structure shown in Figure 24 shows a standing surface wave pattern in both x and y directions with $k_x = 2\pi/L_x$ and $k_y = 2\pi/L_y$. The electron heating also shown in Figure 24 is analogous to the profiles generated in 1d simulations at $p_{argon} = 10mT$. The loop antenna current is higher than might be expected ($\sim 1000amps$ with $L_z = 100.0cm$) because the cavity is operating well below cutoff (to reduce simulation volume) and poor coupling is achieved. This is a purely computational limitation. The device we have modeled could be scaled to larger dimensions by increasing the number of antenae. Standing surface wave plasmas offer large area, low voltage, planar plasmas which are well suited to many plasma processing applications.

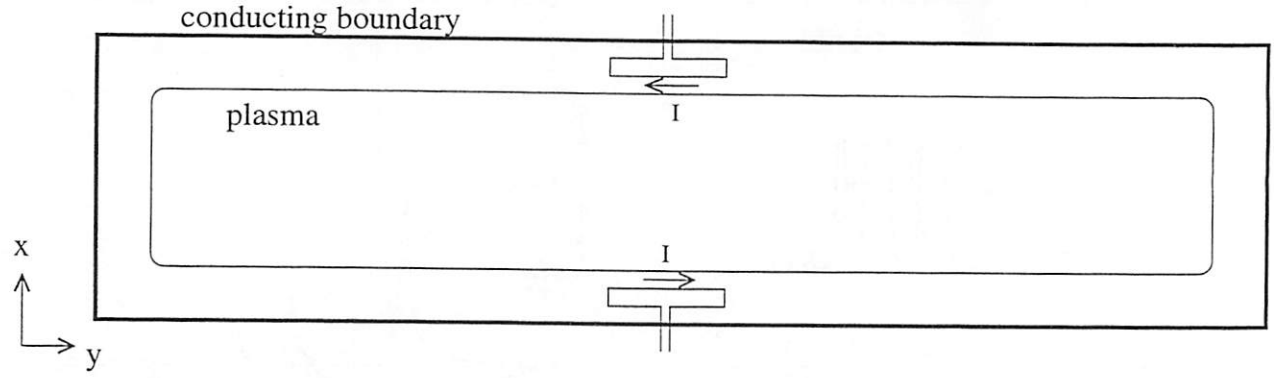

Figure 23: Schematic of 2d model for surface wave sustained discharge.

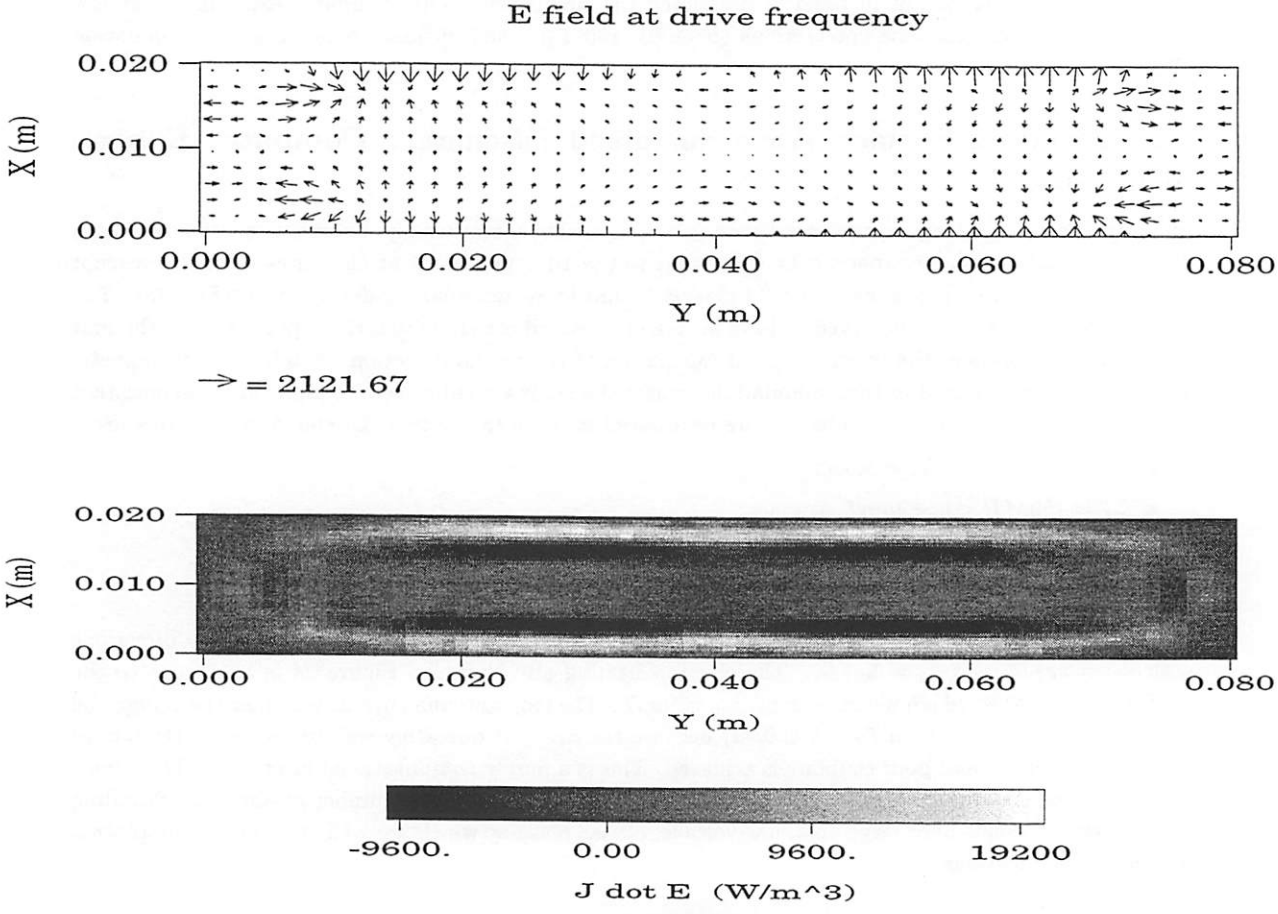

Figure 24: Field structure and heating profile in 2d surface wave sustained discharge.

2 Ion Body Waves

2.1 Observation of Sheath Formation in Bounded Plasma

System 1 is bounded by grounded walls where electrons and ions are absorbed; no secondary electrons are produced. The plasma has no mechanism to maintain itself, therefore it is collected by the walls. The simulation initial condition is with the plasma loaded uniformly with the parameters given in Table 3. In the first few plasma periods enough electrons are absorbed by the wall so that further escape of the electrons are reduced by the positive charge of the ions (ambipolar diffusion). The ions then escape on ion time scales. Figure 25 shows the time history of the decay of the plasma. The contour plot of the average ion velocity is shown in Figure 26. The approach of the sheath into the plasma takes place at close to the sound speed. At later times waves can be seen moving in both directions in Figure 25.

Physical Parameters	Initial electron Temperature	=	$1\ eV$
	Initial Ion Temperature	=	$1 \times 10^{-4}\ eV$
	Initial Center Density	=	$1 \times 10^{14}\ m^{-3}$
	$\frac{Mass of Ion}{Mass of Electron}$	=	1833
	Initial Debye length	=	7.4×10^{-4}m
	Length	=	0.05m
	Length/λ_D	=	67.6
	Initial Electron Plasma Frequency	=	90 MHz
	Initial Ion Plasma Frequency	=	2.1 MHz
Numerical Parameters	Number of cells in x	=	256
	Δ t	=	8.680555×10^{-11} sec

Table 3: Parameters for sheath formation, System 1. See Figures 25 and 26

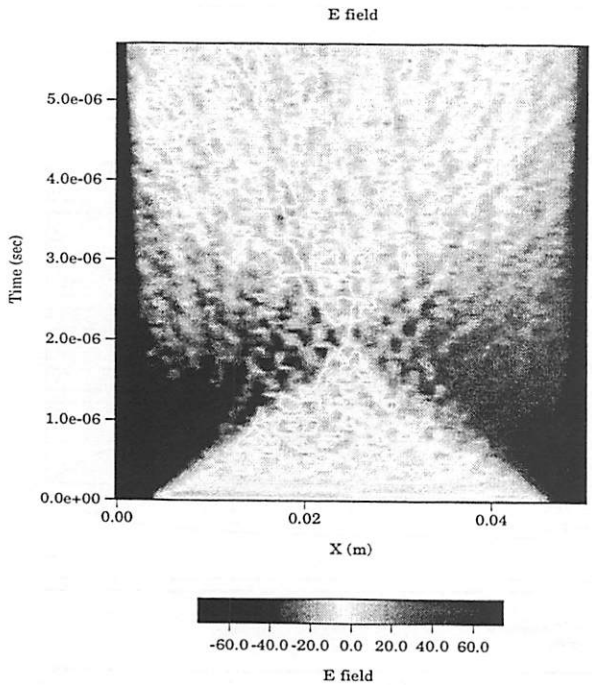

Figure 25: A time history of the electric field showing the sheath collapse.

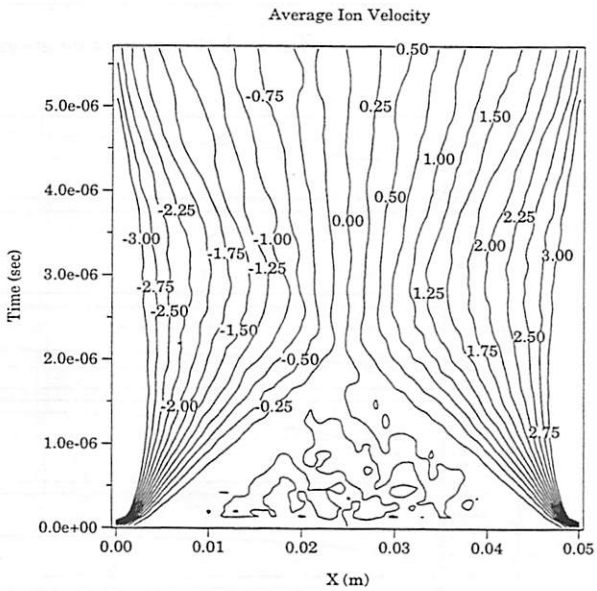

Figure 26: A contour plot of $v(x,t)/v_{sound}(t)$ with $v_{sound}(t) = \sqrt{\frac{T(x=.025m,t)}{m_i}}$. At early times the 0.25 contour is moving inward at $\sim 1.2 v_{sound}$ and the 1.0 contour is moving inward at $\sim 0.86 v_{sound}$.

2.2 Steady State System

System 2 is bounded by grounded walls, where electrons and ion are absorbed when they strike the wall. The parameters are summarized in Table 4. To maintain the plasma, ion - electron pairs are generated in the system at a constant rate uniformly across the system, as if by UV light. The initial condition of this computer experiment is with the simulation region empty. The simulation was run until it reached steady state. Time average spatial profiles of the densities, potentials, and average velocity are shown in Figure 27. The electron and ion phase spaces are shown in Figure 28. Note the position of the sheath, as defined by a common model[10], when the potential drops $T_e/2$, ion average velocity reaches Bohm velocity, and the density is $e^{\frac{-1}{2}}$ of the center density. These all line up in position rather well. The average ion velocity reaches the Bohm velocity closer to the wall than the other two; this is because atoms are being ionized at zero velocity reducing the average ion velocity.

Physical Parameters	Center Electron Temperature	=	2.05 eV
	Center Ion Temperature	=	5×10^{-3} eV
	Center Density	=	2.35×10^{13} m^{-3}
	$\frac{Mass of Ion}{Mass of Electron}$	=	225
	Background gas Pressure	=	3 mTorr
	Ionization rate	=	1.08×10^{16} s^{-1}
	Energy of photon	=	4.51 eV
	mean free path	=	0.16m
	Debye length	=	2.1×10^{-3}m
	Length	=	0.06m
	Length/λ_D	=	28.6
	Electron Plasma Frequency	=	43.6 MHz
	Ion Plasma Frequency	=	2.9 MHz
Numerical Parameters	Number of cells in x	=	512
	Δ t	=	1×10^{-10} sec

Table 4: Parameters for steady state, System 2. See Figures 27 and 28.

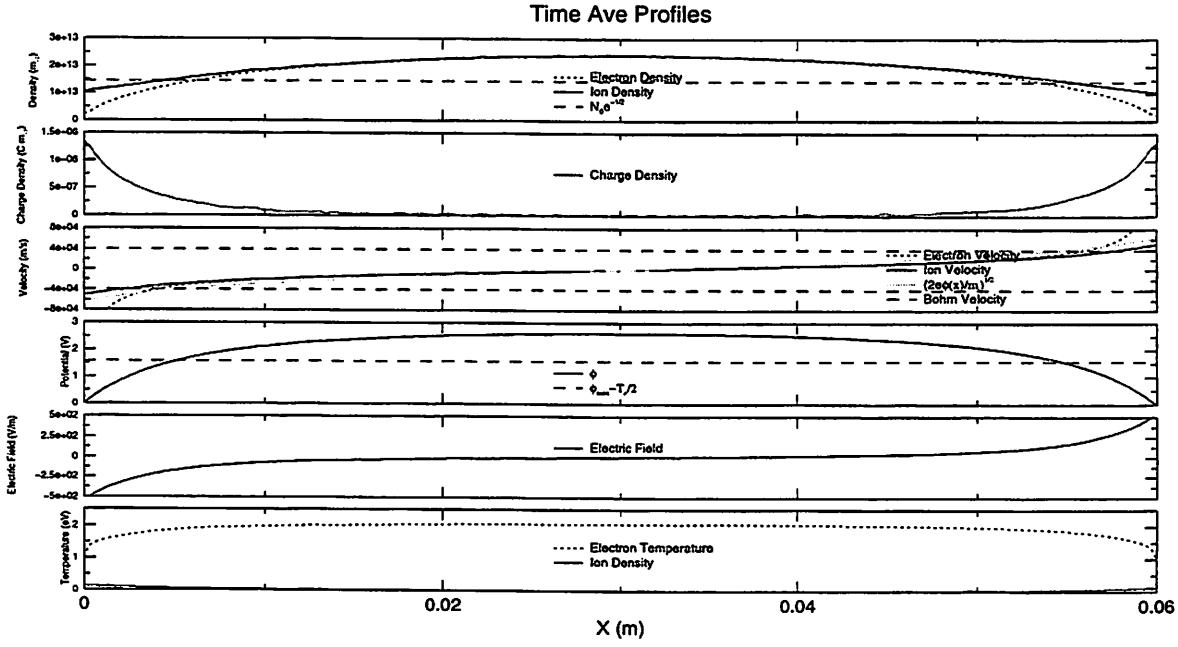

Figure 27: Time average space profiles of the system maintained with photo ionization. Note that the positions of the sheath edge in the density, velocity and potential plots are about the same.

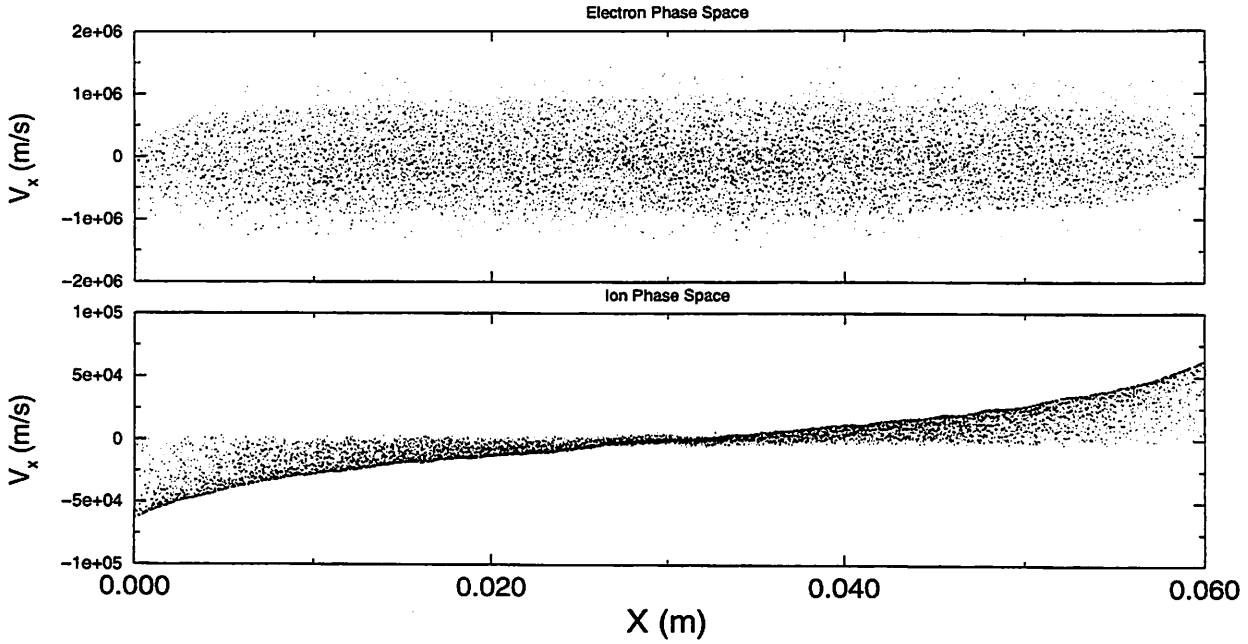

Figure 28: Ion and electron phase spaces of the system maintained with photo ionization. The ion phase space shows distinct ion wave activity.

2.3 Self Excited Waves

A long time ($\sim 143\tau_i$, $\tau_i = 1/f_{pi}$) time history of electric field is shown in Figure 29, for a system similar to that shown in the previous section. The parameters are summarized in Table 5. The time average electric field is subtracted from the instantaneous field in order to obtain Figure 30. This figure shows self excited waves moving in both directions in the bulk of the plasma. The wave crests are not moving at a constant velocity because the background ions have a drift, as shown in Figure 31. Waves that start on the left hand side of the system start with a low velocity as they propagate up stream. These same waves move faster on the right hand side of the system as they are now propagating with the flow direction. The phase velocity of the wave agrees with $\frac{\omega}{k} = \frac{v_{sound}}{\sqrt{1+k^2\lambda_D^2}}$ [11] in the middle of the system where the ion drift velocity is negligible.

Physical Parameters	Center Electron Temperature	=	.931 eV
	Center Ion Temperature	=	5.06×10^{-3} eV
	Center Density	=	8.31×10^{13} m^{-3}
	$\frac{Mass of Ion}{Mass of Electron}$	=	225
	Background gas Pressure	=	3 mTorr
	Ionization rate	=	2.16×10^{16} s^{-1}
	Energy of photon	=	4.51 eV
	mean free path	=	0.15m
	Debye length	=	7.83×10^{-4}m
	Length	=	0.12m
	Length/λ_D	=	153
	Electron Plasma Frequency	=	82.03 MHz
	Ion Plasma Frequency	=	5.5 MHz
Numerical Parameters	Number of cellss in x	=	512
	Δ t	=	2×10^{-10} sec

Table 5: Parameters for the self excited waves, System. See Figures 29, 30 and 31.

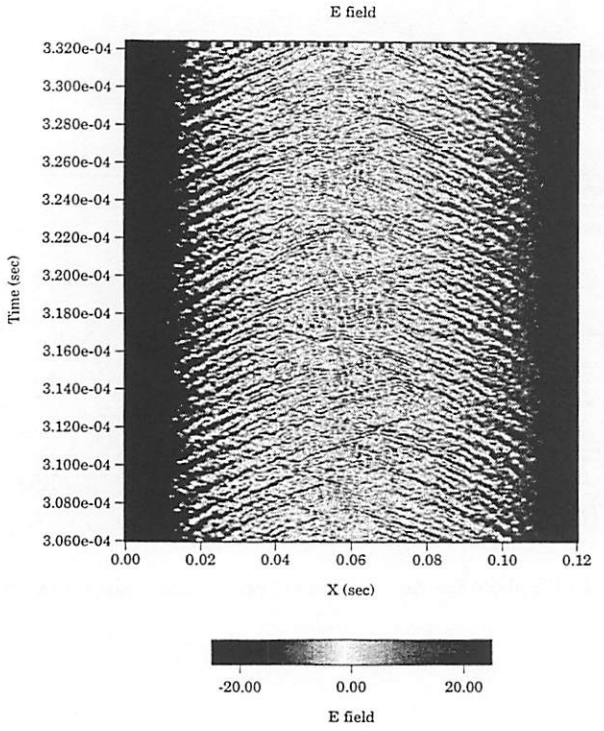

Figure 29: Time history of the electric field in the longer system maintained with photo ionization.

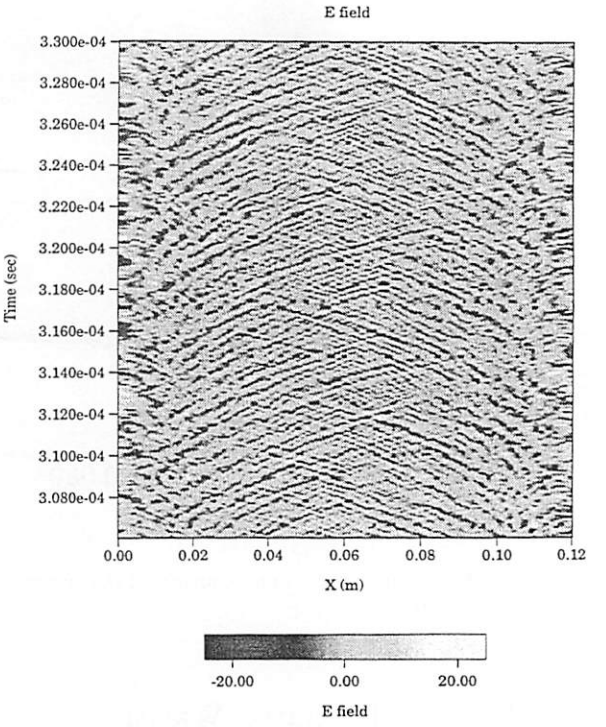

Figure 30: Time history of the electric field perturbation in the longer system maintained with photo ionization.

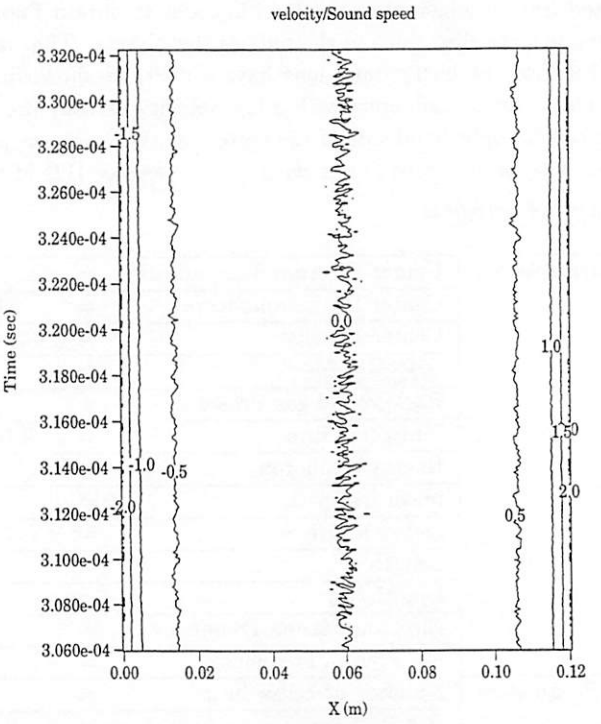

Figure 31: Contour plot of the average velocity of the ions normalized to the sound velocity showing the sheath edge. When this is compared to Figures 29 and 30, the ion waves are seen exist in the bulk of the plasma and not in the sheath region.

2.4 Conclusions

Edge waves and oscillations at high frequencies have been detected in thermally excited metal-bounded plasmas. Ties have been made among many well-known resonances and waves, adding eigenmode structures. Excellent agreement is found between fluid kinetic theory and particle simulations in 1d3v and 2d3v.

These edge waves, beginning with series resonance, have been driven at low voltages (2 and 3 volts) to produce sustained argon discharges, up to densities of about $1 \times 10^{11}\, cm^3$, with density increasing as the cube of the drive frequency. Heating signatures (e.g., $J \cdot E$) are much different than for other discharges; heating mechanisms are yet to be clearly identified.

Sheath formation, starting from a uniform plasma, proceeds at sound speed, followed by trapping of ion sound waves in the center plasma. We observe time-average density, potential and drift velocities to be more or less as expected from elementary analytic models, in both one and two-walled simulations. We have also observed reflection and transmission of ion sound waves (solitons) off of the edge/sheath region. The ties between these waves and sheath, pre-sheath stability are yet to be clarified.

Acknowledgments

This research is supported by ONR grants N00014-90-J-1198, N00014-93-1-1389, and N00014-94-1-1033.

References

[1] J. C. Nickel J. V. Parker and R. W. Gould. Resonance oscillations in a hot nonuniform plasma. *Phys. Fluids*, 7:1489, 1964.

[2] J. Taillet. Resonance-sustained radio frequency discharges. *Amer. J. Phys.*, 37(4):423, 1969.

[3] M. Moisan and Z. Zakrzewski. Plasma sources based on the propagation of electromagnetic surface waves. *J. Phys. D: Appl. Phys.*, 24:1025, 1991.

[4] V. Vahedi X. Q. Xu, G. DiPeso and C. K. Birdsall. Theory and simulation of plasma sheath waves. *Electronics Research Lab*, UCB/ERL M92/148, 1992.

[5] C. C. Cheng and E. G. Harris. Waves and instabilities in a finite plasma. *Phys. Fluids*, 12(6):1262, 1968.

[6] A. W. Trivelpiece and R. W. Gould. Space charge waves in cylindrical plasma columns. *J. Appl. Phys.*, 30:1784, 1959.

[7] R. W. Gould B. O'Brien and J. Parker. Longitudinal wave-propagation modes along a positive column. *Phys. Rev. Letters*, 14:630, 1965.

[8] V. Vahedi and M. Surendra. A monte carlo collision model for the particle-in-cell method: applications to argon and oxygen discharges. *Comp. Phys. Comm.*, 87:179, 1995.

[9] V. A. Godyak. *Soviet RF Discharge Research.* Delphic Assoc., 1986.

[10] M. A. Lieberman and A. J. Lichtenberg. *Principles of Plasma Discharges and Materials Processing.* Wiley, New York, 1994.

[11] F. F. Chen. *Introduction to Plasma Physics and Controlled Fusion.* Plenum Press, New York, 1984.